The Astrophysical Journal, 743:190 (18pp), 2011 December 20 doi:10.1088/0004-637X/743/2/190

ON THE POSSIBLE MECHANISMS OF TWO GROUND-LEVEL ENHANCEMENT EVENTS

Kazi A. Firoz[1], Y.-J. Moon[2,3], S.-H. Park[4], K. Kudela[5], Jamal N. Islam[1], and Lev I. Dorman[6,7]
[1] Research Centre for Mathematical and Physical Sciences, University of Chittagong, 4331 Chittagong, Bangladesh
[2] School of Space Research, Kyung Hee University, 446-701 yongin-si Gyeonggi-do, Republic of Korea
[3] NASA Goddard Space Flight Center, Greenbelt, MD, USA
[4] Solar and Space Weather Research Group, Korea Astronomy and Space Science Institute, 305-348 Daejeon, Republic of Korea
[5] Institute of Experimental Physics, Slovak Academy of Sciences, 04001 Kosice, Slovak Republic
[6] Cosmic Ray Department, Russian Academy of Sciences, N. V. Pushkov IZMIRAN, Troitsk 142190, Moscow, Russia
[7] Cosmic Ray and Space Weather Center, Emilio Segrè Observatory, Technion and Israel Space Agency, Israel
Received 2011 July 1; accepted 2011 August 15; published 2011 December 6

ABSTRACT

We have carried out a case study on the possible mechanism of ground-level enhancement (GLE) occurrence. For this, we have considered two GLE events (GLE69 and GLE70) and scrutinized their relationships with simultaneous soft/hard X-rays as well as solar energetic particle (SEP) fluxes of different energy bands. Although most of the energy bands of the flares maintain strong correlations ($r \geqslant 0.8$) with the GLEs, depending only on this evidence we could not precisely imply that GLEs can be caused by solar flares. So, we have attempted to understand possible relativistic energies of the GLEs, which have been determined by availing the relativistic traversing time and velocities of the particles along the nominal path of Archimedean spiral magnetic field lines. Results suggest that the energy released from accelerated particles in high-energy (γ-ray) solar flares might sometimes cause the GLE. We found that during hard X-ray flares $\leqslant$7 MeV, the relativistic energy ($\leqslant$0.23 GeV) of GLE69 was much less than 1 GeV whereas during SEP flares >30 MeV the possible relativistic energy of GLE69 amounts to ~2.78 GeV, and this makes us believe that GLE69 might be caused by the energy released from particle accelerations in high-energy solar flares. On the contrary, during hard X-ray ($\leqslant$7 MeV) as well as γ-ray solar flares (>30 MeV) the relativistic energy of GLE70 amounts to $\leqslant$~0.35 GeV, indicating that the GLE70 was presumably not caused by the released energy from accelerated particles in the solar flare. Alternatively, the released energy from particle accelerations in solar radio emission type II burst concomitant coronal-mass-ejection-driven shocks seems to have been responsible for causing the GLE70.

Key words: solar–terrestrial relations – Sun: X-rays, gamma rays

Online-only material: color figures

1. INTRODUCTION

Ground-level enhancements (GLEs) represent the largest class of relativistic solar energetic particle (SEP) events $\geqslant$1 GeV produced from some of the most energetic processes, such as solar flares and coronal mass ejections (CMEs), that can convert magnetic energy into kinetic energy (accelerated particles) and thermal energy (heated plasma) on timescales of a fraction of a second to tens of several minutes. The SEPs escaping the solar corona traverse along the Parker (Archimedean) spiral magnetic field lines toward the Earth. The low energetic particles are recorded by satellites at the geostationary orbit, while the high energetic particles are detected by Neutron Monitors on the surface of the Earth. Occasionally, sudden, sharp, and short-lived increases in the intensities of high-energy (GeV) particles are also detected by Neutron Monitors. These increases are known as GLEs. Characteristically, GLEs are different phenomena that can take place across any portion of the solar cycles irrespective of maxima and minima. Details about the historical background and characteristics of GLEs can be studied in a number of papers and books (e.g., Dorman 1957, 1963, 2004, 2006, 2010; Dorman & Miroshnichenko 1968; Cliver et al. 1982; Miroshnichenko 2001; Perez-Peraza et al. 2006; Mavromichalaki et al. 2007; Velinov & Mishev 2008; Bombardieri et al. 2008; Alania et al. 2009).

To identify the responsible solar agent causing a GLE occurrence, several researchers (e.g., El-Borie 2003; Wang & Wang 2006; Cliver 2006; Kane 2009; Firoz et al. 2010) pursued observational studies on the association between GLEs and corresponding solar parameters. Most of the studies commonly suggested that GLE is better associated with a solar flare of strong optical signature and a high-speed CME. However, a few researchers (Firoz et al. 2011a) pointed out that the association does not precisely indicate that GLE can be caused by a solar flare; rather the direct proportionality between the intensive phase of the GLE and the intensive phase of the concurrent solar flare is the main property to investigate for an understanding of the mechanism. This latter view was in line with the report of Aschwanden (2011), who noted that 85% of the GLE events were accelerated during the intensive phases of solar flares and 15% of the GLE events were accelerated by extended acceleration processes (probably by CME-driven shock fronts). To set up a conclusive remark, Firoz et al. (2011b) checked the cross-correlation between intensive phases of GLEs and the corresponding solar flares while reiterating the suggestion that the closer time-integrated solar flare might be the responsible agent.

Earlier, there was a progressive idea proposed by Perez-Peraza et al. (2006, 2008) on the categorization of GLEs into two components such as "prompt GLE" and "delayed GLE." In agreement with the idea, Aschwanden (2011) defined the prompt GLE as caused by flare-accelerated particles in the lower corona, whereas the delayed GLE was more likely produced by particles accelerated in CME-driven shocks during their propagation through the corona and heliosphere. All of these developments seemed to have been in line with Reames (1999)

who defined impulsive (prompt) events as originating from a narrow range of solar longitudes, whereas gradual (delayed) events originate from a broad range of heliolongitudes of CME-driven shocks. This indicates that prompt GLE events might be caused by flares and delayed GLE events by CME-driven shocks. In this context, Firoz et al. (2010) reported that GLE-associated CME properties do not symbolize any particular evidence that can define types of CMEs separately on the prompt and delayed GLE events. To some extent, Firoz et al. (2011a) opined that the CME alone does not create the enhancement in CRI, but the particle accelerations in CME-driven shocks may modulate CRI either directly or inversely. In this regard, it is relevant to note that shock wave acceleration, with optimum parameters (>2000 km s^{-1}), scarcely produces protons of less than 400 MeV (see Berezhko & Taneev 2003). Particles that escape by drifts seldom give rise to the intensity of GLE. Therefore, it is superfluous to emphasize that GLE can be caused by shock waves.

To realize the time integration and correlation between GLEs and solar flares, Firoz et al. (2011b) recently performed a cross-correlation study between GLEs and soft X-ray solar flares and found that most of the GLEs have strong correlations and closer time integration with simultaneous solar flares but that some GLEs did not maintain closer time integrations with the solar flares; hence, it becomes necessary to check the cross-correlations between GLEs and high-energy solar flares. Motivated by these statements, we have again followed the method of cross-correlation and pursued a case study on the relationship between GLE and soft/hard X-ray solar flares of different energy bands and SEP flares of a few energy bands. For better understanding, we have also checked flare properties such as relative solar flux density (s.f.u.), solar emission measure (cm^{-3}), solar energy-loss rate (erg s^{-1}), and temperature (MK). However, we could still not confirm unambiguously that GLE might be caused by solar flares, even though there are strong correlations as well as time integrations between high-energy solar flares and GLEs. So, we have made an extended effort to understand the relativistic energy of GLE. For that, we have determined the relativistic traversing time of the GLE particle by availing the observed time lag and subsequently the possible velocity of the particle in terms of the nominal path lengths obtained by Reames (2009a, 2009b). The traversing time and velocity have been utilized to find possible relativistic energy of GLE. This gives us an opportunity to comprehend that if the relativistic energy is equal to or greater than 1 GeV, the GLE is most likely produced by a solar flare and conversely, if relativistic energy is less than 1 GeV then the GLE is likely produced by another acceleration process (perhaps CME-driven shocks). Thus, we have tried to look into the possible mechanism of GLE production.

2. OBSERVATION, DATA TREATMENT, AND ANALYSIS

2.1. Ground-level Enhancement

In order to understand the possible mechanism of GLE occurrence, we have investigated relationships and time integrations of GLEs with soft/hard as well as SEP flares. For this, based on the availability of the data of hard X-ray flares, we are able to study a few events, GLE64 through GLE70 for the period of 2002–2006. We preferred data of cosmic ray intensity (CRI) from the Oulu Neutron Monitor (ONM)[8] because it has the desired higher resolution of 1 minute time-cadence pressure-corrected data (higher resolution data show GLE more precisely than lower resolution data do). Instrumentation of the ONM has been reviewed in Firoz et al. (2010).

To examine the increase rate of the CRI of each GLE event, we followed the theorem and mathematical expressions illustrated in previous articles (Firoz et al. 2011a, 2011b). Finally, we decided to concentrate on GLE events[9] that have a peak increase rate >10% because, for the event where the signal is less than 10%, the onset is not well determined as only the peak intensity is seen above the background. On the basis of this criterion, we have only two events (GLE69 and GLE70) with a peak increase rate >10%, so we decided to pursue a case study with these two events that may be considered as a model for statistical studies in the future.

For both events we considered a time window over 8 hr (480 minutes) covering phases of impulsive courses (waveforms) and background signals (see Figures 1(a) and (b)). In GLE69, intensive phase and background signals of the time window cover 06:00:00 through 13:59:59 (UT). In GLE70, intensive phase and background signals of the time window cover 00:00:00 through 07:59:59 (UT). The intensive phase of the GLE69 event is observed at a time of 06:50–8:00 UT and the intensive phase of the GLE70 event is observed at a time of 02:30–3:20 UT. Note that we defined the start time and the onset time of each event such that the "start time" was earlier than the "onset time"—the start time is the time when the event is about to take place, whereas the onset time is the time when the intensity begins rising from its background level. Accordingly, the start time, onset time, and peak time of GLE69 and GLE70 and their associated solar flares of different energy bands have been noted in Tables 2 and 3. These tables help us look into the differences in start, onset, and peak times of the different energy bands and to see the differences with GLE69 and GLE70 at a glance. The principle aim of these tables is to compare the peak time differences observationally to determine the length of the time integration between flare and GLE.

To see the consistency of the data, we checked the amplitude, phase, and dispersion of the data by means of the least-squares method (Firoz & Kudela 2007; Firoz 2008). Analysis of the difference between GLE and a GLE-event has been presented in the recent study of Firoz et al. (2011b), whereas variations of non-GLE cosmic rays have been examined in perspective of the paradigm (Firoz et al. 2009). Since a GLE is a highly anisotropic event, the effects of longitudinal or latitudinal differences with respect to various sites of neutron monitors may sometimes vary the CRI and this issue has already been analyzed by several researchers (e.g., Plainaki et al. 2007; Mavromichalaki et al. 2010).

2.2. Solar Flare

A solar flare generates radiation across the electromagnetic spectrum at various wavelengths. The radiation observed at soft X-ray energies is typically at thermal (10^{o}–30^{o} MK) bremsstrahlung whereas hard X-rays are at both thermal (10^{o}–30^{o} MK) and non-thermal (>30^{o} MK) bremsstrahlung. Hard X-rays are high-energy fluxes and soft X-rays are comparatively referred to as low-energy fluxes. Detailed analyses of

[8] Oulu Neutron Monitor (ONM): (http://oldcr.oulu.fi).

[9] Ground Level Enhancement (GLE): (http://cosmicrays.oulu.fi/GLE.html).

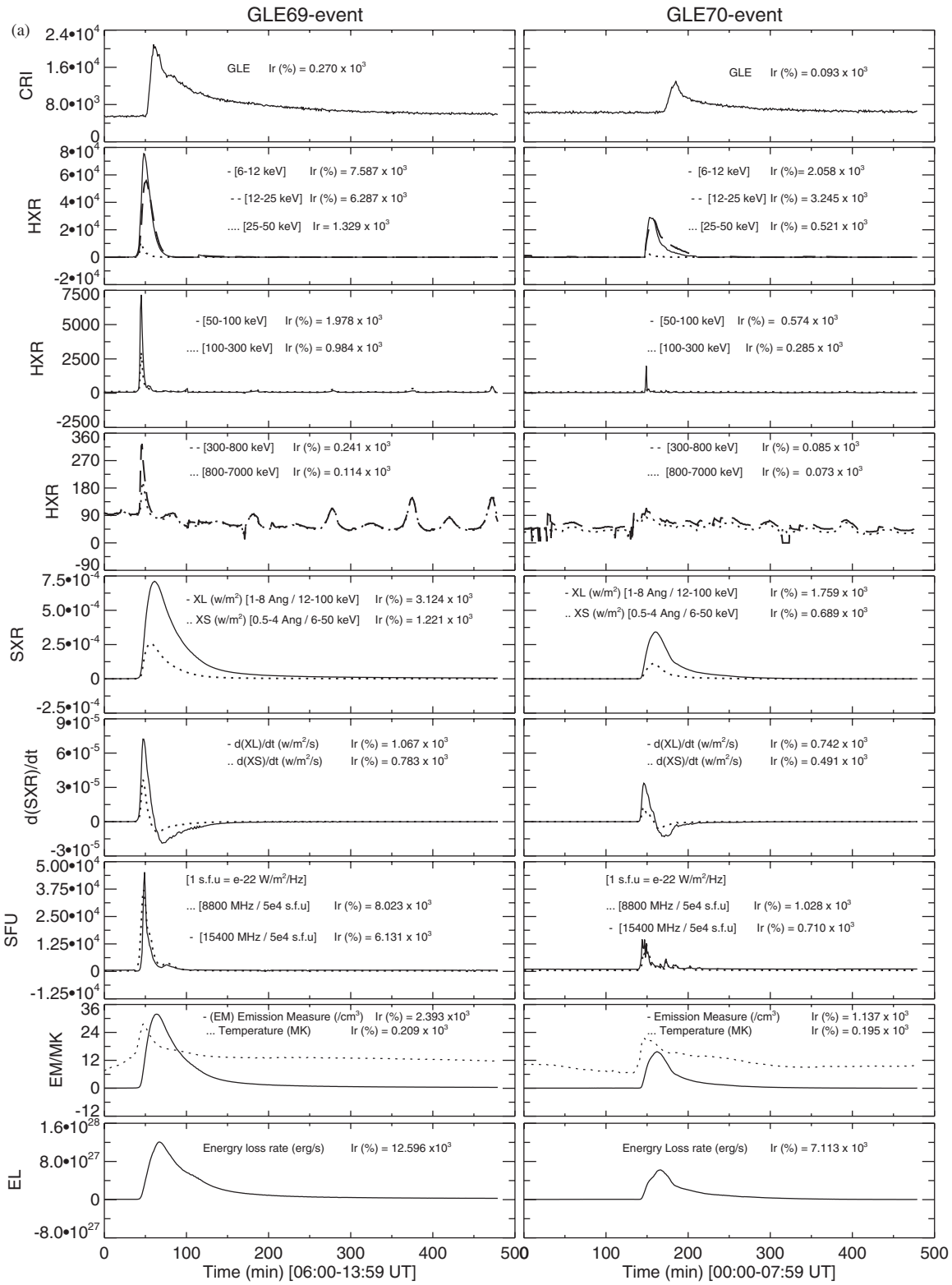

Figure 1. (a) Time profiles of the CRI of GLE69 and GLE70 are compiled with concurrent (i) hard X-rays (HXR) within energy bands 6–12 keV, 12–25 keV, 25–50 keV, 50–100 keV, 100–300 keV, 300–800 keV, 800–7000 keV; (ii) the soft X-rays (SXR) and their derivative forms of longer wavelength (1–8 Å) and shorter wavelength (0.5–4 Å) within energy bands <25 keV; (iii) the solar radio flux density (SFU); (iv) the emission measure (EM; cm^{-3}), temperature (MK), and energy-loss rate (EL; erg s^{-1}) of the solar flares. Increase rates (I_r %) of all solar parameters displaying a comparison picture from the perspective of enhancement between GLE69 and GLE70 have been deduced by means of the equation proposed earlier by Firoz et al. (2011b). (b) GLE69- and GLE70-associated SEP data of the energies >30 MeV, >50 MeV, and >100 MeV are exhibited. Based on the availability of the data, we took the 5 minute resolution of SEP from *GOES*10 (*Yohkoh*: (http://solar.physics.montana.edu/sxt/)) for the energy channels >30 MeV, >50 MeV, and >100 MeV (cm^{-2} str^{-1} s^{-1}) and composed with the same resolution of 5 minute time-cadence CRI data for the GLE69 and GLE70 events.

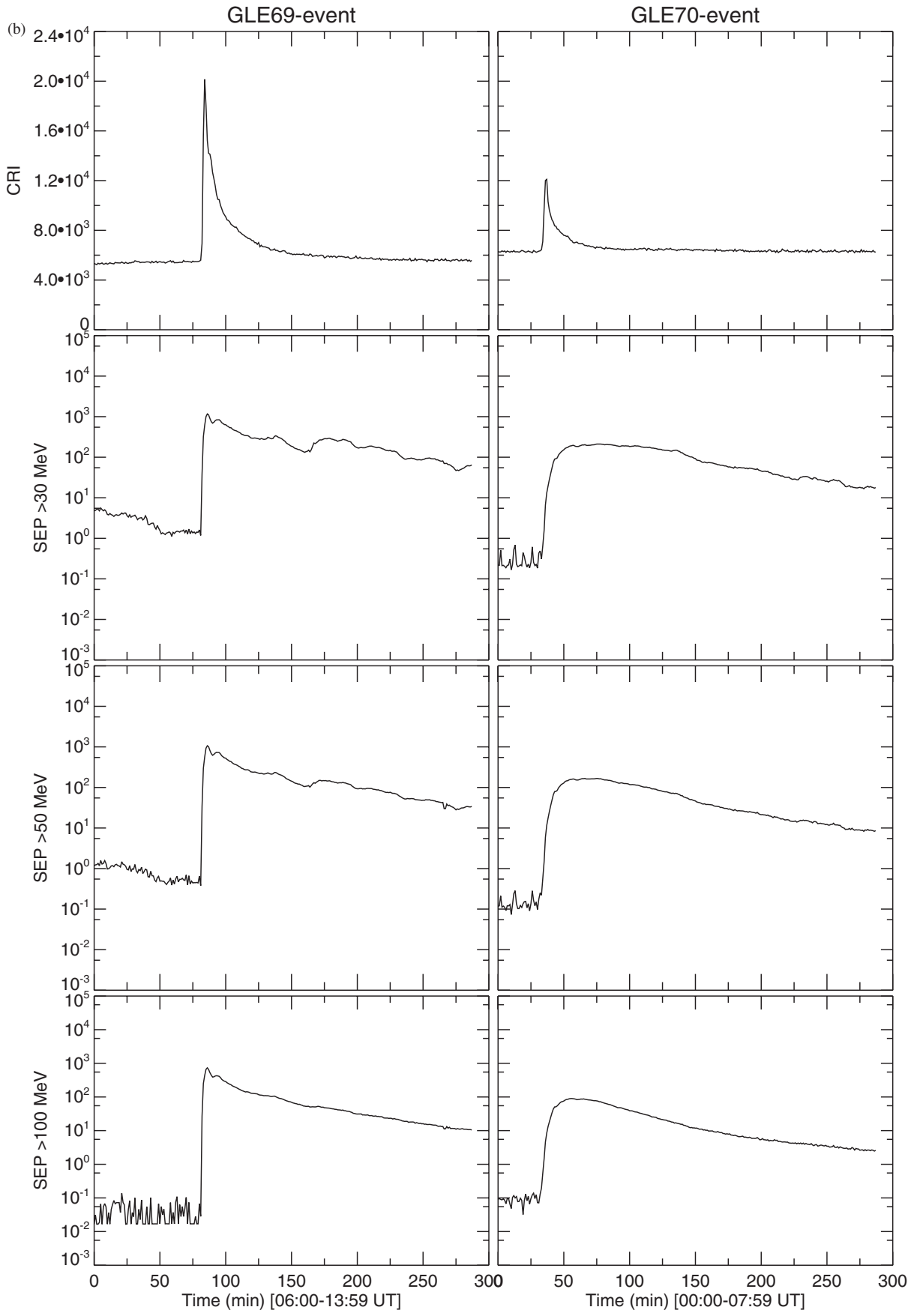

Figure 1. (Continued)

the difference between soft and hard X-rays were performed in the papers Dennis (1985) and Veronig et al. (2002).

Hard X-rays within energy bands ∼<25 keV are also considered in the soft X-ray range of *GOES* where shorter wavelengths are between 0.5 Å (∼24.84 keV) and 4 Å (∼3.13 keV) and longer wavelengths are between 1 Å (∼12.42 keV) and 8 Å (∼1.5 keV). It is also clear that the derivative part of the intensive phase of soft X-ray fluxes within energy bands ∼<25 keV is almost simultaneous with the intensive phase of the hard X-ray fluxes (Figure 1(a)), and this indicates that the accelerated electrons generate the soft X-rays, which obey the Neupert effect (Neupert 1968; Warren & Antiochos 2004).

Because the relationship between soft X-ray solar flares and GLE has been interpreted in the recent study of Firoz et al. (2011b), in this work, we feel necessary to study the relationship between GLE and different components of solar flares in order to comprehend which sort of solar flare is more effective in possible GLE production. For this purpose, based on the availability of the resolution, we used the soft/hard X-ray of 1 minute time cadence and SEP of 5 minute time cadence (see Figures 1(a) and (b)).

2.2.1. Soft X-Ray Flux

We used the data of the solar soft X-ray fluxes (W m^{-2}), energy-loss rates (erg s^{-1}), emissions (cm^{-3}), and temperature (MK) for the abundance spectral model Coronal Chianti 6.0.1. The data have been retrieved under the workbench of SSW for the satellite *GOES*12 archived in *Yohkoh*.[10] (Instrumentation of *GOES*12[11] and data of soft X-ray fluxes have been introduced earlier in Firoz et al. 2011b). We processed the data of X-ray fluxes over bands XL (longer wavelength 1–8 Å at ∼12–1.5 keV) and XS (shorter wavelength 0.5–4 Å at ∼24.84–3.13 keV) with gain change spikes smoothed out in W m^{-2}.

2.2.2. Hard X-Ray Flux

For hard X-ray fluxes, we employed the data of *RHESSI*[12] (Lin et al. 2002; Dennis et al. 2005) which uses a single instrument measuring high-energy X-ray emissions at different energies. *RHESSI* is designed to image solar flares in energetic photons from soft X-rays (∼3 keV) to γ-rays (∼20 MeV). Here, the light curves for hard X-ray fluxes we utilized are of seven different energy bands (thermal: 6–12 keV, non-thermal: high sensitivity in the energy range of 12–25 keV, 25–50 keV, 50–100 keV, 100–300 keV, 300–800 keV, 800–7000 keV) belonging to the wavelengths ∼2.07 Å to ∼0.0018 Å. The data are just the rates in each of the germanium detectors as a function of time with a time resolution of 4 s that is approximately the spin period of the spacecraft. The data of 4 s time cadence have been averaged into the resolution of 1 minute time cadence. These data have been composed with the same resolution of 1 minute time-cadence CRI of GLE69 and GLE70 (see Figure 1(a)).[9–14]

2.2.3. Gamma-Ray Emission

Gamma- (γ) rays are high-frequency electromagnetic radiation. The neutral pions which are produced during the acceleration of protons to higher energies can produce high-energy gamma-rays through the decay process. The presence of protons accelerated in the solar atmosphere is defined by the remarkable plateau in the energy range 25–100 MeV of the γ-ray emission spectra. Details about the relationships between γ-ray flares and high-energy particles have been given in several papers (Ryan et al. 2000; Chupp et al. 2003; Kuznetsov et al. 2006; Kurt et al. 2010). Thus, strong correlation between peaks of GLE and SEP flux can indicate a good correlation between GLE and γ-rays, and due to the unavailability of γ-ray data, as an alternative, we have considered SEP fluxes to study with GLE events.

Based on the availability of the data, we took the 5 minute resolution data of SEP from *GOES*10[10] for the energy channels >30 MeV, >50 MeV, and >100 MeV (cm^{-2} str^{-1} s^{-1}) and composed with the same resolution of 5 minute time-cadence data of GLE69 and GLE70 (see Figure 1(b)). Instrumentation of *GOES*10 has been briefed in the recent study (Firoz et al. 2011b).

2.3. Relative Solar Radio Flux Density

When a solar flare erupts, noise from the flare is received over a wide range of frequencies. The amount of solar noises/the radio wavelengths emitted by the Sun is measured as solar flux units (s.f.u., 1 s.f.u. = 10^{-22} W^{-1} m^{-2} Hz^{-1}). The 1 s time cadence of solar radio flux data has been taken from Learmonth solar telescopes preserved at the RSTN[14] and averaged into 1 minute time cadence. Although the Learmonth solar radio telescopes monitor both the quiet and active Sun, we took the data during the active Sun into account because solar flares are believed to occur during the active Sun. The origin of the solar noise corresponding to higher frequency (8800 MHz/15400 MHz) in lower chromospheres is supposed to be concerned with the solar flares. This is why we chose the solar flux units for the frequencies of 8800 MHz and 15400 MHz for better understanding of the GLE-associated solar flares (see Figure 1(a)).

2.4. Solar Radio Burst

Solar radio bursts (types I–V) are generated by electron streams as they propagate along magnetic field lines from solar corona to interplanetary medium. Generally solar radio burst type III is associated with high-energy solar flare and type II is associated with a CME-driven shock wave (fundamentally, type II represents the signatures of coronal shocks). For both types of solar radio bursts, the emission mechanism is a plasma process where electron beam energy subsequently converts into a propagating electromagnetic wave (Wild et al. 1963; Aschwanden 2006; MacDowall et al. 2009). Therefore, it is necessary to understand how the radio emission bursts originated from the GLE69- and GLE70-associated solar flares. For this purpose, we processed the data recorded by *WIND*–WAVES[15] (Cane & Erickson 2003; Reiner et al. 2007).

2.5. Coronal Mass Ejection

Ejections of huge bubbles of magnetized gas of thermal energy from the Sun are known as CMEs. These CMEs are observed by LASCO on board *SOHO*. It is believed that particle accelerations take place in the CMEs, which may induce the enhancement of CRI. Hence, we

[10] *Yohkoh*: 1 (http://solar.physics.montana.edu/sxt/).
[11] *Geostationary Operational Environmental Satellite* (*GOES*): http://goes.ngdc.noaa.gov/)
[12] *RHESSI*: (http://hesperia.gsfc.nasa.gov/rhessidatacenter/)
[13] National Geophysical Data Center (NGDC): (http://www.ngdc.noaa.gov/)
[14] Radio Solar Telescope Network (RSTN): (http://www.ngdc.noaa.gov/stp/solar/solarradio.html).
[15] *WIND*-WAVES: (http://lep694.gsfc.nasa.gov/waves).

Table 1
The Cross-correlations of GLE69 and GLE70 with Flare Components

Flare Components	Solar Flare										Relative Solar Radio Flux Density (SFU)			
	EM (cm^{-3})		EL ($erg\ s^{-1}$)		Temperature (MK)		Derivative (longer wavelength) soft X-Ray (dX_L/dt)		Derivative (shorter wavelength) soft X-Ray (dX_S/dt)		8.8 GHz		15.4 GHz	
	R_{gem}	dT_{gem} (minutes)	R_{gel}	dT_{gel} (minutes)	R_{gtem}	dT_{gtem} (minutes)	R_{gdxl}	dT_{gdxl} (minutes)	R_{gdxs}	dT_{gdxs} (minutes)	$R_{s.f.u.4}$	$dT_{s.f.u.4}$ (minutes)	$R_{s.f.u.}$	$dT_{s.f.u.}$ (minutes)
GLE69	0.95	16	0.86	13	0.99	14	0.99	13	0.98	14	0.99	13	0.99	12
GLE70	0.96	22	0.97	19	0.92	34	0.96	35	0.97	36	0.98	36	0.97	36

Notes. 1st column: the highest correlations and corresponding time lags of GLE69 and GLE70 with concurrent emission measure (EM), energy loss rate (EL), and temperature of the solar flare and derivatives of soft X-ray flares are noted. The cross-correlations and time lags of soft X-rays for longer wavelengths (X_L) and shorter wavelengths (X_S) have been found exactly the same as found before in Firoz et al. (2011b). 2nd column: the highest correlations and time lags of GLE69 and GLE70 with concurrent relative solar flux units (8.8 GHz and 15.4 GHz) are also noted.

Table 2
Start, Onset, and Peak Time of the GLE69- and GLE70-associated Hard X-Ray Solar Flares of the Energy Bands of 6–12 keV, 12–25 keV and 25–50 keV

GLE				HXR (6–12 keV)					HXR (12–25 keV)					HXR (25–50 keV)				
Flare Component	Start (UT)	Onset (UT)	Peak (UT)	Start (UT)	Onset (UT)	Peak (UT)	dT_{ob12} (minutes)	dT_{st12} (minutes)	Start (UT)	Onset (UT)	Peak (UT)	dT_{ob25} (minutes)	dT_{st25} (minutes)	Start (UT)	Onset (UT)	Peak (UT)	dT_{ob50} (minutes)	dT_{st50} (minutes)
GLE69	6:50	6:56	7:01	6:20	6:40	6:51	9	11	06:36	06:42	06:48	12	13	06:39	06:43	06:45	15	15
GLE70	2:50	2:58	3:05	2:28	2:34	2:38	27	27	02:28	02:31	02:33	32	28	02:28	02:31	02:33	33	33

Notes. Time lags between peaks of those GLEs and concurrent solar flares of those bands, observationally (dT_{ob}) as well as statistically (dT_{st}), are noted. The highest correlations and these time lags are displayed in Figure 4.

Table 3
Start, Onset, and Peak Time of the GLE69- and GLE70-associated Hard X-Ray Solar Flares of the Energy Bands of 50–100 keV, 100–300 keV, 300–800 keV, and 800–7000 keV

HXR (50–100 keV)					HXR (100–300 keV)					HXR (300–800 keV)					HXR (800–7000 keV)				
Start (UT)	Onset (UT)	Peak (UT)	dT_{ob100} (minutes)	dT_{st100} (minutes)	Start (UT)	Onset (UT)	Peak (UT)	dT_{ob300} (minutes)	dT_{st300} (minutes)	Start (UT)	Onset (UT)	Peak (UT)	dT_{ob800} (minutes)	dT_{st800} (minutes)	Start (UT)	Onset (UT)	Peak (UT)	dT_{ob7k} (minutes)	dT_{st7k} (minutes)
6:38	6:43	6:45	15	16	6:38	6:44	6:45	15	16	6:41	6:44	6:46	14	15	6:41	6:44	6:46	14	14
2:26	2:28	2:29	36	35	2:27	2:28	2:29	36	36	2:29	2:27	2:28	36	32	02:50	2:58	3:05	51	46

Note. Time lags between peaks of those GLEs and concurrent solar flares of those bands, observationally (dT_{ob}) as well as statistically (dT_{st}), noted here are displayed in Figure 4. The highest correlations detected at these time-lags are also displayed in Figure 4. Figure 4 and Tables 2–3 present a collective picture to see the comparison at a glance.

examined properties (speed, angular width, central position angle, height, etc.) and images of GLE69- and GLE70-associated CMEs observed by LASCO C2 and C3[16] (Yashiro et al. 2004). We have employed the usual data of CME events associated with those two GLE events. (Contiguous time-series data of CMEs are not available, hence it is not possible to examine CMEs at both growth and decay phases of the GLE). Timings of the CME-driven shock waves have been set up in terms of the solar emission type II radio bursts.

3. METHODOLOY

3.1. Cross-correlation and Time Lag

Since there is a time difference observationally between a solar flare and a GLE, important information can further be drawn by looking into the statistical time lag. The time lag is at the course (waveform) of the phase where the strongest correlation exists. For this purpose, we considered the cross-correlation theorem, and verified time-lags between courses of the intensive phases of GLE events and the intensive phases of hard X-rays/soft X-rays (flux intensity, emission measure, energy-loss rate, etc.) as well as SEP flares of a few energy bands. First, we fixed the peak of GLE, with respect to which we searched the strongest correlative point of the course along the intensive phase of the solar flare. One example is exhibited in Figure 3(a) for a hard X-ray flare and another example is in Figure 3(b) for an SEP flare. The durations of the intensive phases are assumed as boundaries within which the highest correlations have been searched. The time shifted within the boundaries varies between 1 and 12 minutes, but often the strongest correlations have been detected at the wave points between 3 and 6 minutes. Thus, the time lags have been considered at the wave points where the strongest cross-correlations were detected. The methodology and process of the cross-correlation as well as determination of the time lag followed in this study have been explained in our recent paper (Firoz et al. 2011b).

Although it is difficult to precisely pinpoint the peak time based on the time lags from the perspective of cross-correlations, they can be compared with observational analysis for better understanding. Usually, the strongest correlations are found between the peaks of the intensive phases of the two time series, but at times the strongest correlations are also found at a point close to the peak point along the growth or beginning points of decay phases. This is why, at times, there is a difference in time lags obtained statistically and observationally that has been explained earlier in Firoz et al. (2011b). Here, we have also noted the observational and statistical time lags for each energy band of solar flares (see Tables 2 and 3).

3.2. Relativistic Velocity and Energy of a GLE Particle

Particles erupted from the Sun usually move outward along the interplanetary magnetic field lines following nominal paths of the Archimedean spiral magnetic field. Thus, a GLE particle traverses along spiral magnetic field lines while the light from the Sun traverses straight to the Earth. If we can estimate the time of the traversed particle that must be more than the time taken by the light of the Sun, we can ultimately learn the velocity of the particle. Based on this point of view, the recent study of Firoz et al. (2011b) recognized the possible relativistic time and velocity of the particle with respect to the observational time lag between peaks of the GLE and solar flare. Accordingly, the possible relativistic velocity of the traversing GLE particle along the spiral magnetic field lines yields as follows:

$$v_p = \frac{l_p}{\left(\Delta t + \frac{l_c}{c}\right)}, \tag{1}$$

where Δt is the time lag that gives the traversing time of the GLE particle as $t_p = \Delta t + t_c$ and l_p is the nominal path length between the Sun and the Earth along the Archimedean spiral magnetic field lines supposed to be traversed by the GLE particle with velocity v_p (velocity of the GLE particle is considered invariant throughout the path). The length l_c is the distance between the Sun and the Earth traveled by the light with velocity c. By virtue of Equation (1), we can find a presumable relative particle velocity and then check the possible time taken by the particle.

Using the onset times of different ions of different energy bands for a GLE event, it is possible to estimate the distance traveled by particles prior to their arrival at a spacecraft and to infer the release time from the Sun. Accordingly, the path lengths $l_p = 1.19 \pm 0.02$ AU and $l_p = 1.72 \pm 0.05$ AU traversed by GLE69 and GLE70 particles, respectively, along the spiral field lines were deduced by Reames (2009a, 2009b). Taking these path lengths into account, we determined the possible velocities of GLE69 and GLE70 particles by means of Equation (1). It is clear that if the path length is higher, the relativistic velocity would be higher thereby giving rise to the relativistic energy of GLE. When we have the velocities of the GLE particles for different energy bands of solar flares, we deduce the relativistic energies of the GLE particles with respect to each band of solar flares by utilizing the following equation:

$$E_g = \gamma m_p c^2 - m_p c^2 = \left[\frac{1}{\sqrt{1 - \left(\frac{v_p}{c}\right)^2}} - 1\right] m_p c^2, \tag{2}$$

where E_g is the relativistic kinetic energy of the GLE particle, m_p is the rest mass of the particle ($m_p c^2 = 938.27$ MeV), v_p is the velocity of the particle determined by Equation (1), and c is the velocity of the light. For each energy band of the flares, we have a peak time difference between the GLE and flare that can be used to deduce the possible traversing time and velocity of the GLE particle along the spiral field lines. The particle velocity has then been used to obtain the relativistic energy of the GLE by means of Equation (2).

By employing Equation (2), one can also check the velocity of the solar flare particle for each energy channel as follows:

$$v_f = c\sqrt{1 - \frac{1}{\left(1 + \frac{E_f}{m_p c^2}\right)^2}} \quad (\text{km s}^{-1}) \tag{3a}$$

or

$$v_f = 0.12\sqrt{1 - \frac{1}{\left(1 + \frac{E_f}{m_p c^2}\right)^2}} \quad (\text{AU minute}^{-1}), \tag{3b}$$

where 1 AU $= 1.5 \times 10^8$ km (approx.) and E_f is the relativistic energy for different energy channels of the solar flares. These equations are also consistent with the suggestion of Aschwanden (2011).

[16] Coordinated Data Analysis Workshop (CDAW): (http://cdaw.gsfc.nasa.gov/CME_list/).

4. RESULTS AND DISCUSSION

4.1. General Trend of the Components of Solar Flares during GLE69 and GLE70

Figures 1(a) and (b). The intensities of GLE69 and GLE70 are seen varying with respect to the intensities of all components. The intensity of GLE69 is almost three times that of GLE70 and this trend is more or less followed by all components of solar flares. The characteristic is also supported by the emission measure, temperature, and energy-loss rate of the solar flare. This indicates that all of these species originated from the same immensely solar eruptive episodes. The radio wavelengths display significant variations in the flux profiles (SFU), in which the sharp rise denotes that the gyrosynchrotron emissions were generated by the accelerated electrons at the reconnection site of the GLE69-associated solar flare and this suggests the presence of a strong responding radio burst concomitant high-energy solar flare. Something similar occurred for the GLE70-associated solar flare with much less magnitude. Although there were double peaks at the GLE70-associated radio wavelengths, there were no strong quasi-periodic oscillations. They otherwise indicate that there were no strong modulations by magnetohydrodynamic or nonlinear relaxation oscillations of wave–particle interactions (e.g., Kumar et al. 2010).

Furthermore, we note that the intensive phase of the solar flare is more closely time-integrated with the intensive phase of GLE69 than with that of GLE70. Thus, we find that the stronger enhancement in a GLE event is directly proportional to the stronger increment of the intensive phase of the solar flares. This is also consistent with the earlier suggestion (Firoz et al. 2011a) that the direct proportionality of the closer time-integrated rising portion of intensive phases of GLE and solar flares is the main concern for understanding the mechanism. However, the same energy band of solar flares at a different time has a different increment in the intensive phase which we can see in these two events. This implies that the closer the time integration is, the greater the effectiveness might be of the released energy from the solar flare to cause enhancement in CRI.

4.2. Difference between GLE69- and GLE70-associated Solar Flares

According to the observation recorded in Solar Monitor[17] (Gallagher et al. 2002), the GLE69-associated solar flare with simple magnetic configuration ($\beta\delta/\beta\gamma$) originated from the northwest active region (N14W61), whereas the GLE70-associated flare with a complex magnetic configuration ($\beta\gamma\delta/\beta\gamma\delta$), consisting of a mixture of polarities in a dominantly bipolar structure originated from the southwest active region (S06W23) of the Sun. In another respect, it is observed that the active region (N14W61) of the GLE69-associated solar flare was nearly at the sub-solar point, near the Sun–Earth connecting magnetic field lines through which energy released from flare-accelerated particles may easily pass along the nominal spiral field lines. By contrast, the active region (S06W23) of the GLE70-associated solar flare was about 40° away from the sub-solar point, away from the Sun–Earth connecting magnetic field lines, and the energy released from the flare-accelerated particles might not be passed through spiral field lines smoothly. This finding is partially compatible with that of Bombardieri et al. (2008) who observed that the location of the X-ray and γ-ray emission (N14W61) was near Sun–Earth connecting magnetic field lines. This can be noticed in the distribution of active regions on the Sun recorded in Solar Monitor (globe figure in Firoz et al. 2011b also has evidence). Therefore, the possibility of the production of GLE69 by solar flare is much higher than that of GLE70.

[17] Solar Monitor: (http://www.solarmonitor.org).

4.3. Solar Radio Burst during GLE69 and GLE70

Figures 2(a) and (b). As observed, the intensive phase (∼06:40–7:20 UT) of the GLE69-associated solar flare corresponded to the most rapid responding phase (06:50–07:10 UT) of the obvious solar radio type III burst, which flourished >400 kHz and decayed from ∼400 kHz to ∼100 kHz until 08:30 (UT). It is consistent with the solar radio emission, which starts rising from 06:48 (UT) through 07:04 (UT) and then starts decaying (see Figure 1(a)). Thus, the most rapid response to the particle acceleration phase is found associated with the solar radio type III burst that appears as long as the intensive phase of the hard X-ray flare emission exists. Otherwise, the presence of the radio type III burst suggests the existence of opening magnetic field lines (e.g., Aschwanden et al. 1995; MacDowall et al. 2003). The energy released from flare-accelerated particles transmitted along the Earth-connected field lines via those open magnetic field lines might cause enhancement in CRI.

The peak of GLE69 is at ∼07:01 UT, which is ∼03 s later than the radio type III burst and concomitant hard X-ray flares. It signifies that the flare-released energy closely induced the GLE occurrence. Similarly, we verified the profile of the solar radio burst which corresponded to the intensive phase (∼02:30–03:00 UT) of the GLE70-associated solar flare—we noticed that there was also a solar radio type III burst with less complexity at ∼02:28 UT to ∼03:00 UT across when there seemed to have been stronger emissions of type II burst and extended weaker emissions are also visible over the decay phase of the flare.

The peak of the GLE70 is at ∼03:05 UT, which is ∼15 s later than the concurrent type III burst, and it signifies that the flare-released energy seldom induces the occurrence of GLE70. The GLE69-associated type III burst is more closely time-integrated than the GLE70-associated type III burst and the induction by the flare-accelerated particle on GLE69 is much stronger than that of GLE70. The remarkable difference between the GLE69-associated solar radio type III burst and the GLE70-associated solar radio type III burst is that the GLE69-associated radio type III burst is more pronounced, dynamic, wider, and more closely time-integrated than the GLE70-associated radio type III burst, whereas the GLE70-associated type II burst is more pronounced, dynamic, and extended than that of GLE69. The conclusion drawn from this is that GLE69 might be the particle intensified by the energy released from a solar flare, whereas GLE70 might be the particle intensified by the energy released from a CME-driven shock. Another thing that is visible is that there seems to have been small-scale CME–CME interaction in the interplanetary medium before the GLE70-associated type III burst and this was not visible before the GLE69-associated type III burst.

4.4. CME-driven Shock Concomitant Type II Burst during GLE69 and GLE70

The GLE69-associated CME speed (882 km s^{-1}) is much slower than the GLE70-associated CME speed (1773 km s^{-1}). The fast CME is generally accompanied by shock waves, but a

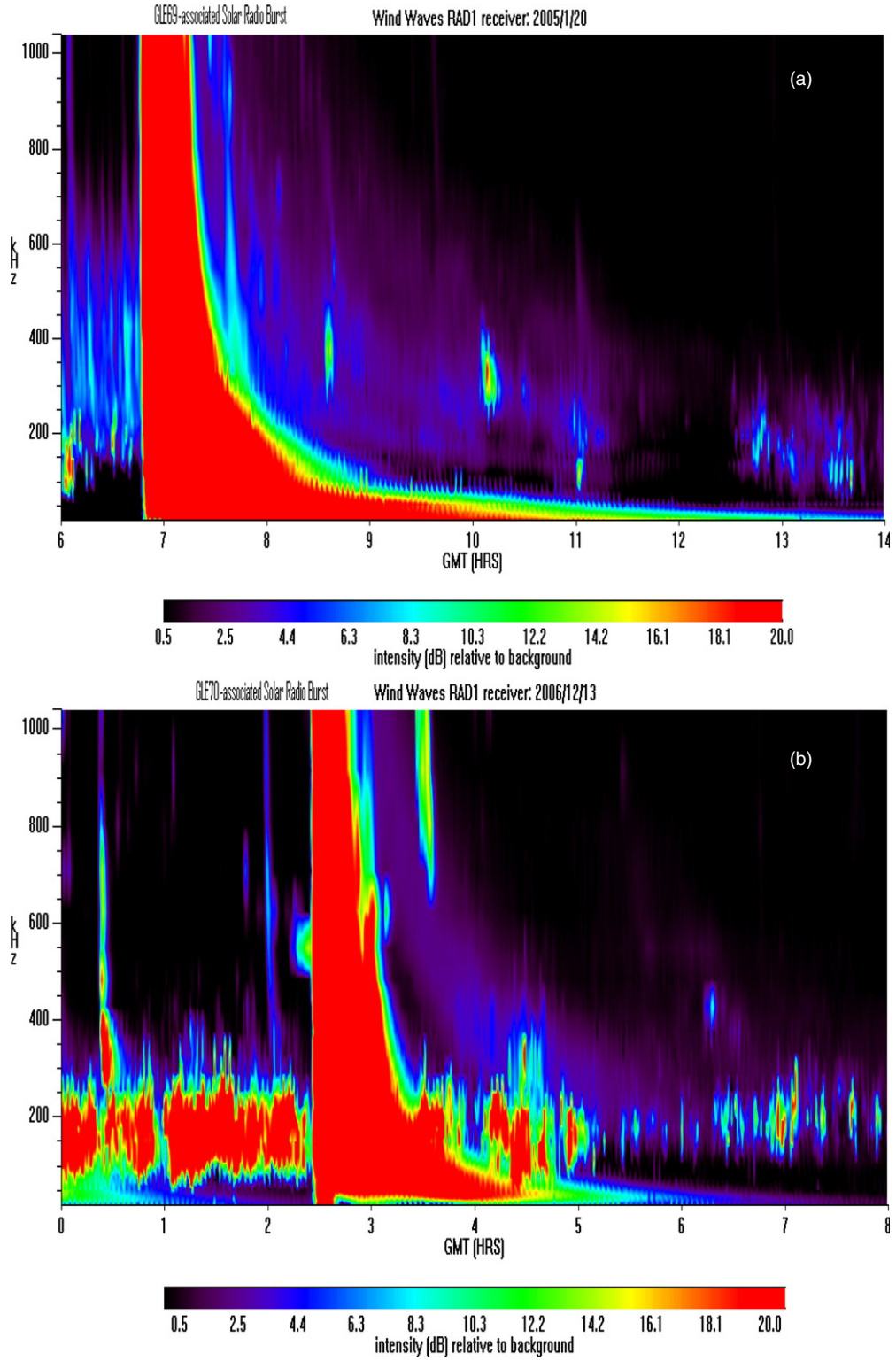

Figure 2. (a) Solar radio burst that took place during the intensive phase of the GLE69-associated soft/hard X-ray flares. Here, we can see that there is a type III radio burst that naturally associates with a hard X-ray flare. The type II radio burst concomitant shock wave seems to be less dynamic along the decay phase of the GLE69-associated flare than along that of GLE70-associated flare. The radio emission bursts that originated from the GLE69- and GLE70-associated solar flares have been processed in *WIND*–WAVES (http://lep694.gsfc.nasa.gov/waves). (b) The solar radio burst that took place during the intensive phase of the GLE70-associated soft/hard X-ray flares. Here, we can see that there is a type III radio burst that naturally associates with a hard X-ray flare. The type II radio burst concomitant shock wave seems to be more dynamic along the decay phase of the GLE70-associated flare than along that of the GLE69-associated flare. The radio emission bursts that originated from the GLE69- and GLE70-associated solar flares have been processed in *WIND*–WAVES (http://lep694.gsfc.nasa.gov/waves).

(A color version of this figure is available in the online journal.)

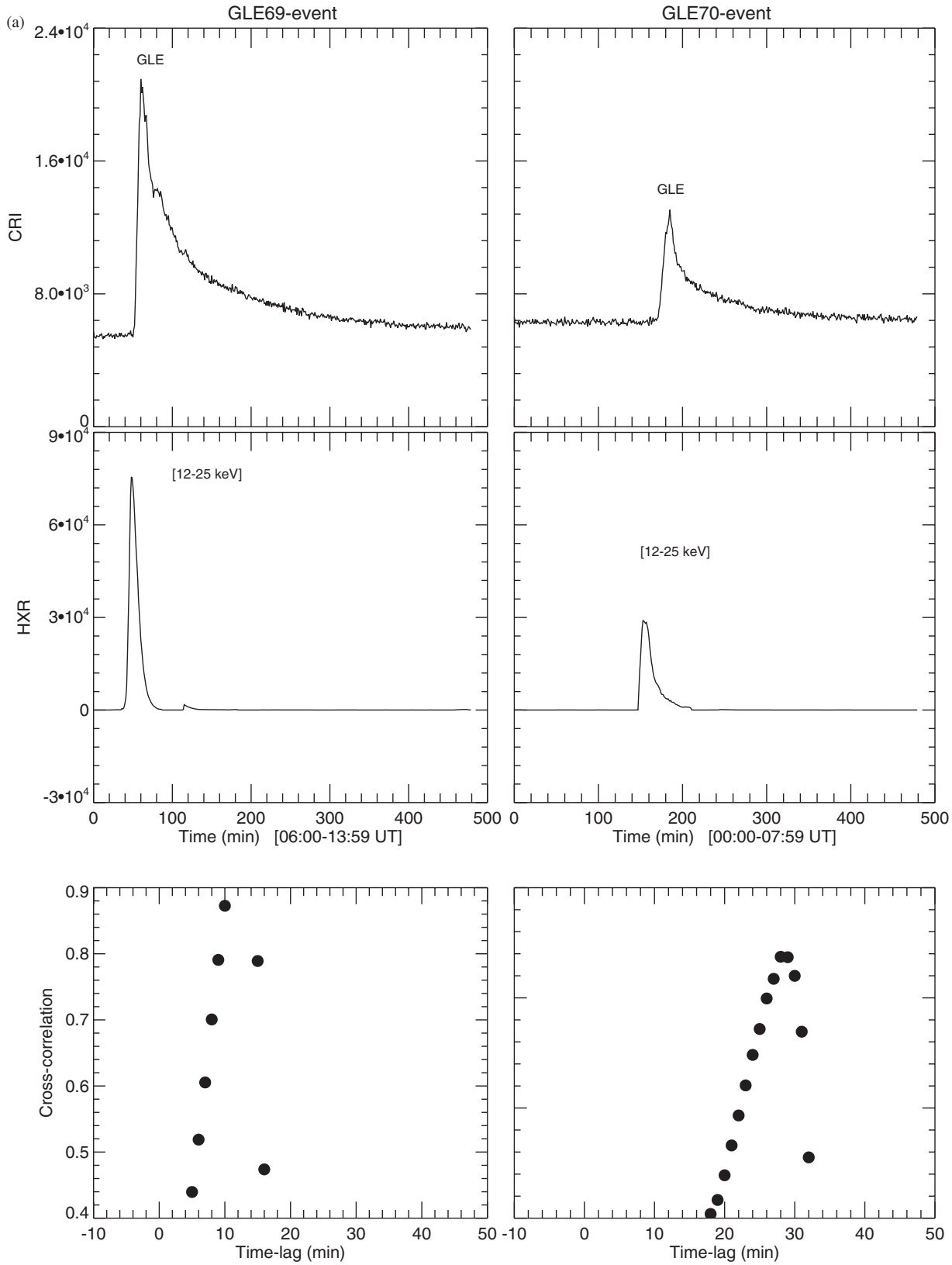

Figure 3. (a) Top: CRI profiles of the events of GLE69 and GLE70 compiled simultaneously (mid) with hard X-ray flux (HXR) of energy band 12–25 keV, over the time windows of 06:00:00–13:59:59 UT (GLE69) and 00:00:00–07:59:59 UT (GLE70) of 1 minute time cadence, maintain (bottom) different correlations at different time lags. The highest correlation and its corresponding time-lag have been taken into consideration.(b) Top: CRI profiles of the events of GLE69 and GLE70 compiled simultaneously (mid) with SEP (>100 MeV), over the time windows of 06:00–13:55 UT (GLE69) and 00:00:00–07:59:59 UT (GLE70) of 5 minute time cadence, maintain (bottom) different correlations at different time lags. The highest correlation and its corresponding time lag have been taken into consideration.

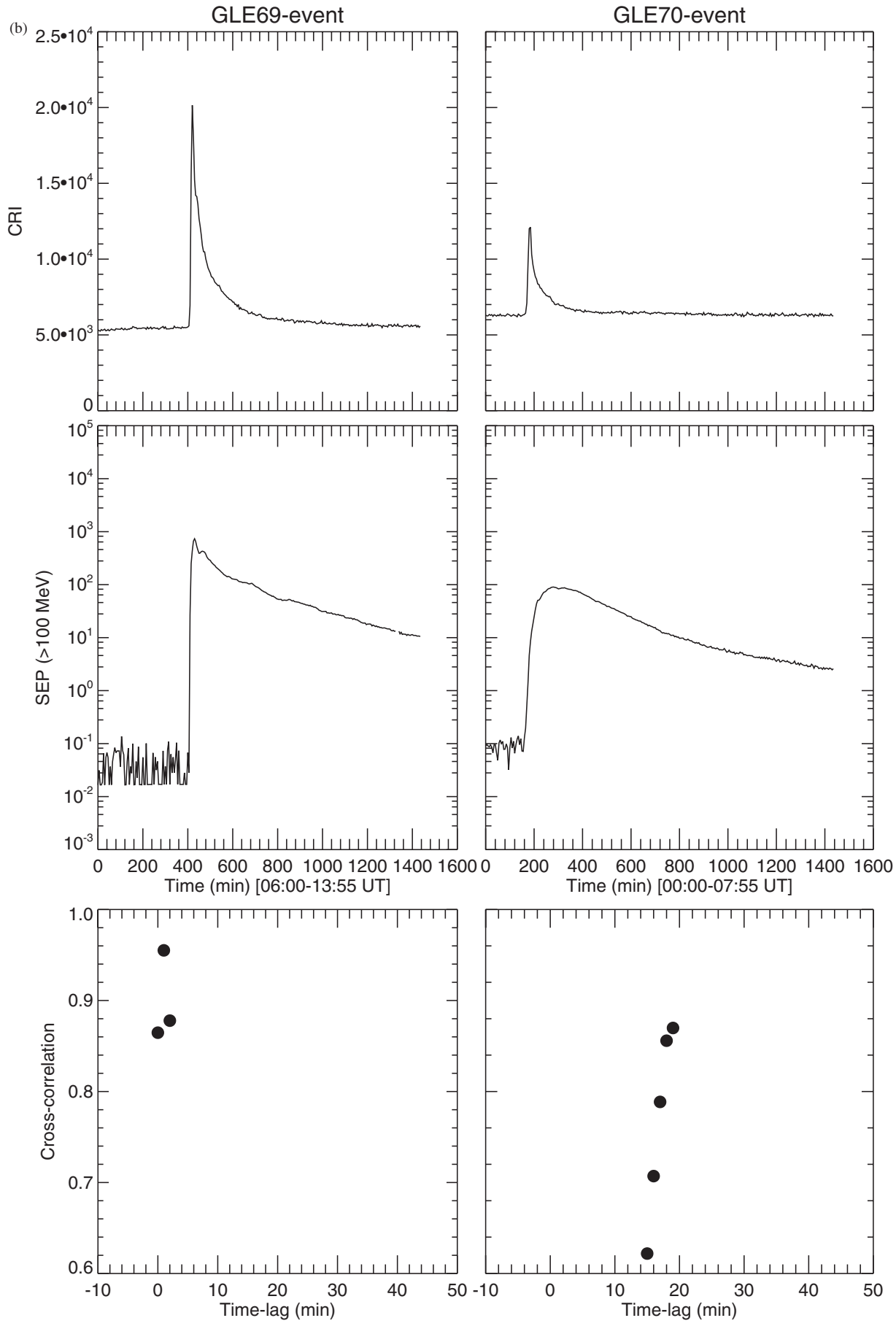

Figure 3. (Continued)

type II radio emission burst is also associated with CME-driven shocks. (In fact, type II radio bursts are thought to be an indicator of the presence of fast and wide CMEs (Wang et al. 2006)). So, the faster the CME is, the faster the type II emission burst will be and hence the possibility of the impact of a CME-driven shock on GLE70 is consequently greater than the possibility of its impact on GLE69. As seen in Figures 2(a) and (b), along the decaying phase (∼400 kHz to ∼100 kHz) of the GLE69-associated type III emission burst, there were some frequency-drifting type II emissions generated by the propagation of the CME-driven shock waves. The GLE69-associated shock concomitant type II burst seems to be much less dynamic than that of the GLE70 and it can be assumed that the particle acceleration during GLE70 was generated in the CME-driven shock front.

Although GLE is associated with the fast CME, it does not precisely imply that it can cause the enhancement in CRI (explanation in Firoz et al. 2010). All properties of CMEs are to be considered to understand the possibility of the occurrence. For example, the central position angle of the GLE69-associated CME is much wider than that of the GLE70-associated CME (see Table 4). For better comprehension, we have exhibited GLE69- and GLE70-associated EIT images (see Figures 6(a) and (b) recorded by WAVES; Moon et al. 2002).[15] Upon investigating the images, it is found that the GLE69-associated CME (apparently ejected from behind the limb of the Sun) was 30° high directed at the north, whereas the GLE70-associated CME was 23° high directed at the south.

Another aspect is that the fast and wide CMEs have an important role in the production of large SEPs (explanation in Kahler et al. 2001). The SEP event often corresponds to the CME-driven shock concomitant type II burst, and it is found that the GLE69 did not have a corresponding SEP event, whereas GLE70 did (see Table 4). As seen in Figure 2(b), onsets of the radio II burst preceded the GLE70 onset times, indicating that the mechanism accelerating high-energy relativistic particles is probably CME-driven shocks (e.g., Kahler et al. 2003; Reames & Lal 2010).

4.5. Relationship of GLE69 and GLE70 to Solar Flares

Figures 3(a) and (b), and 4. Within the shortest time lag (<16 minutes), GLE69 maintains the strongest correlations with soft/hard X-ray flares (6–100 keV), whereas, except for hard X-rays (50–100 keV), GLE70 maintains the strongest correlations with all soft X-ray flares (⩾8 Å) and all hard X-ray flares (6–50 keV) over longer time lags (>23 minutes). On an average, the cross-correlation (0.95) between GLE69 and hard X-ray flares is slightly more than the cross-correlation (0.93) between GLE70 and hard X-ray flares. It implies that the closer time-integrated rising phase of soft/hard X-ray fluxes might induce GLE (the energy released from the hard spectra of closer solar flare might contribute to the production of GLE). The cross-correlations of GLE69 and GLE70 with soft X-rays are exactly the same as those from earlier results (see Firoz et al. 2010). From the perspective of the previous study (Firoz et al. 2011a) in which the relationships of GLEs with various solar parameters have been checked, we are now convinced that GLE is much better correlated with solar flares than with any other solar agents.

Since the derivative form of the intensive phase of the soft X-rays corresponds to the simultaneous intensive phase of the hard X-rays, we also checked the cross-correlation and time lag between the intensive phase of hard X-rays (⩽8 Å/⩽100 keV) and the derivative form of the intensive phase of soft X-rays (⩽8 Å). On average, the cross-correlation between the derivative form of soft X-rays and GLE is almost similar to the cross-correlation between the hard X-rays and GLE. Flare properties (solar flux density, emission measure, temperature) also have good correlations following the trends of solar soft/hard X-ray flares (see Table 1 and Figure 4). To an extent, we found that SEP flares >30 MeV maintained the least time lag, thereby evolving relativistic energy >1 GeV for GLE69. The GLE70 maintains longer time lag with γ-ray flares >30 MeV, which evolves less than 1 GeV, and therefore much higher energy SEP flares may be checked for confirmation. (Most probably, all of the energy bands for SEP flares have an almost similar pattern, with an intensity difference like that seen for three energy bands in Figure 1(b), so GLE70 might be caused by another particle acceleration process such as a CME-driven shock). In line with Aschwanden (2011), we can assume that the GLE having an observational time lag between 2 and 10 minutes with a concurrent flare is a "prompt GLE" and the one with a greater time lag is a "delayed GLE." Accordingly, GLE69 is a prompt GLE and GLE70 is a delayed GLE.

Results of the cross-correlations between GLE and the derivative form of soft X-rays implied almost similar results to that of the cross-correlations between GLE and hard X-rays (see Figure 4 and Table 1). The results of the cross-correlations and time lags between GLE and soft X-rays for longer wavelengths X_L and shorter wavelengths X_S have been found to be exactly the same as found previously (Firoz et al. 2011b). On the basis of the results of cross-correlations of hard X-ray and soft X-ray fluxes with concomitant GLE, we suggest that GLE might be induced by both soft and hard X-ray flares. This means that GLE might be induced by the released energies from closer time-integrated solar flares of different wavelengths. We guess that some of the particles presumably undergo trajectories owing to the interactions with magnetospheric field and conserve energies in each step of the trajectories in the magnetosphere before being incident onto Earth's surface (e.g., Kudela & Usoskin 2004; Firoz 2006), and hence the GLE measured on Earth's surface may not be the same as the actual enhancement in near-geostationary as well as in near-Earth space.

4.6. Possible Relativistic Energies of GLE69 and GLE70

Figure 5. If the released energy from the solar flare is responsible for the sudden enhancement in CRI then we can believe that the closer the time integration between the solar flare and GLE is, the greater the impact of the energy released from the solar flare on GLEs should be. Under this condition, seeing the strong correlation and closer time integration between peaks of GLE and the corresponding solar flare, we can consider that GLE might be induced by the released energy of the solar flare. A different hard X-ray flare has a different energy band and the flare that has the closest time integration also has the best correlation. The closer time-integrated phases of the GLE and flare also display higher speeds of GLE, and subsequently higher relativistic energy of GLE. This suggestion comes from the results of cross-correlations and time lags (Figure 4) and relativistic speeds and energies of GLE69 and GLE70.

We can see (Figure 5) that the GLE69 might be caused by the released energy from SEP flares because it maintains the strongest correlations with the lowest time lag and higher relativistic particle energy. This evidence is also supported by

Table 4
GLE69- and GLE70-concurrent Solar Erupted Events

GLE				CME					Radio type II burst				Emission	SEP event		
									On Figures 2(a)–(b)		On NOAA[a]		*RHESSI*			
Flare Components	Start (UT)	Onset (UT)	Peak (UT)	T_{fap} (UT)	P.A. (°)	Rs (°)	V_{cme} (km s^{-1})	AW (°)	Start (UT)	End (UT)	Start (UT)	End (UT)	EM (cm^{-3})	Start (UT)	End (UT)	Location
GLE69	6:50	6:56	7:01	06:54	290	30 N	882.1	360	06:46	07:22	06:44	07:00	18.70	-	-	-
GLE70	2:50	2:58	3:05	02:54	193	23 S	1773.7	360	02:30	02:52	02:26	02:44	12.03	03:10	09:25	S05W23

Notes. GLE69- and GLE70-associated: (1st column) CME first appearance time (T_{fap}), position angle (P.A.), height (Rs), velocity (V_{cme}), angular width (AW); (2nd column) the start and end time of the CME-driven shock-associated type II burst. (The start time and end time of the GLE69- and GLE70-associated type II burst based on CULG/LEAR differs from what can be seen in the images (Figures 2(a) and (b)) recorded by *WIND*–WAVES. The mean of the 1 minute resolution data of emission measure is also given to understand the overall emission status.) The last column is the GLE70-corresponding solar energetic particle (SEP) event ("-" denotes no SEP event corresponding to GLE69).

[a] National Oceanic and Atmospheric Administration (NOAA): (ftp://ftp.ngdc.noaa.gov/STP/SOLAR_DATA/SOLAR_RADIO).

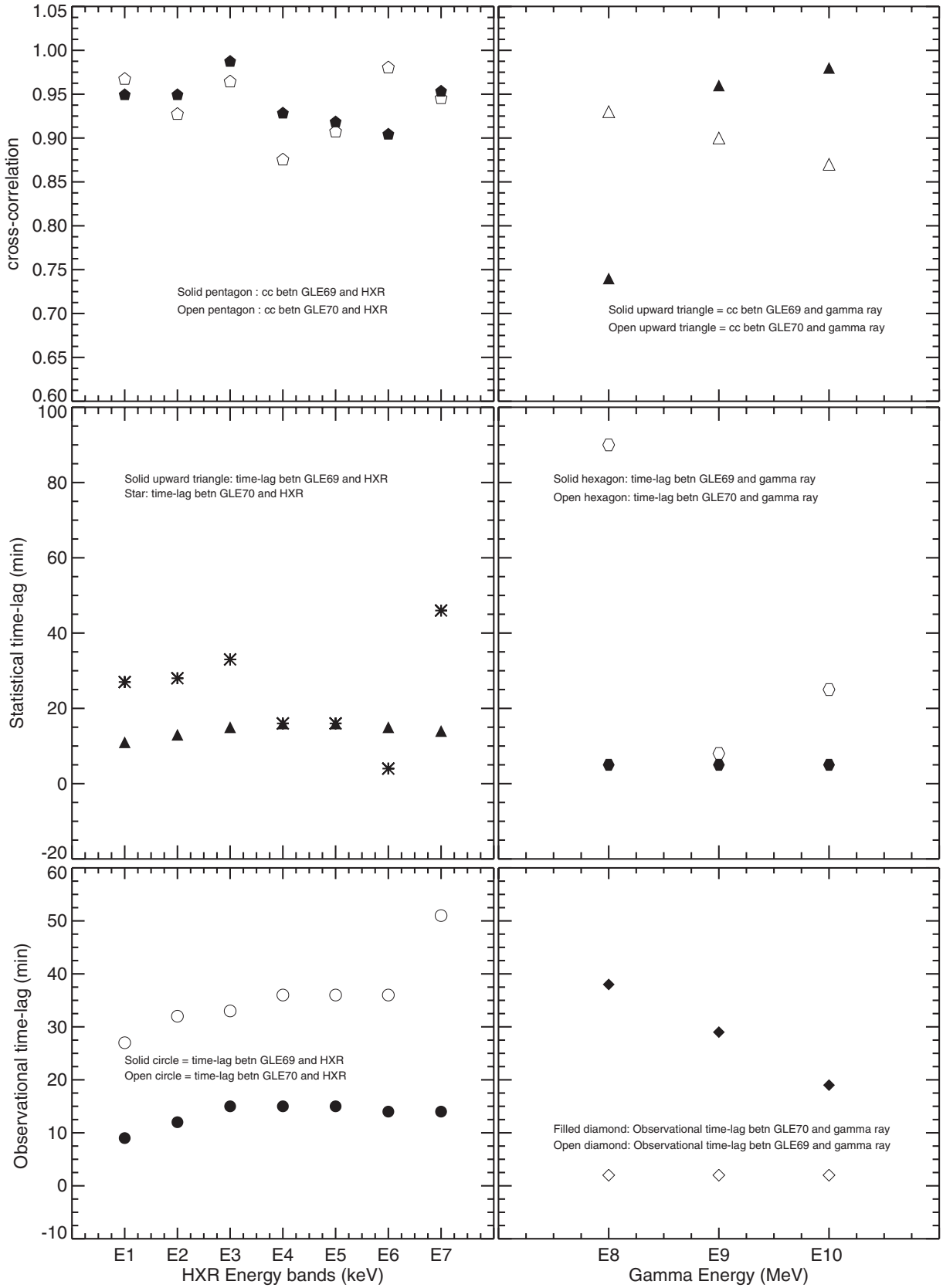

Figure 4. First column: cross-correlations (top) and corresponding time lags (mid) of GLE69 and GLE70 and with concurrent hard X-ray fluxes ($E_1 = 6$–12 keV, $E_2 =$ 12–25 keV, $E_3 = 25$–50 keV, $E_4 = 50$–100 keV, $E_5 = 100$–300 keV, $E_6 = 300$–800 keV, $E_7 = 800$–7000 keV), and time difference between peaks of GLE69/GLE70 and those hard X-ray flares are distributed as functions of the energy bands. Second column: cross-correlations (top) of GLE69 and GLE70 with the SEP flares ($E_8 =$ >30 MeV, $E_9 = >50$ MeV, and $E_{10} = >100$ MeV (cm^{-2} str^{-1} s^{-1})) with GLE69/GLE70 and statistical time lags (mid) and the observational time lags between peaks (bottom).

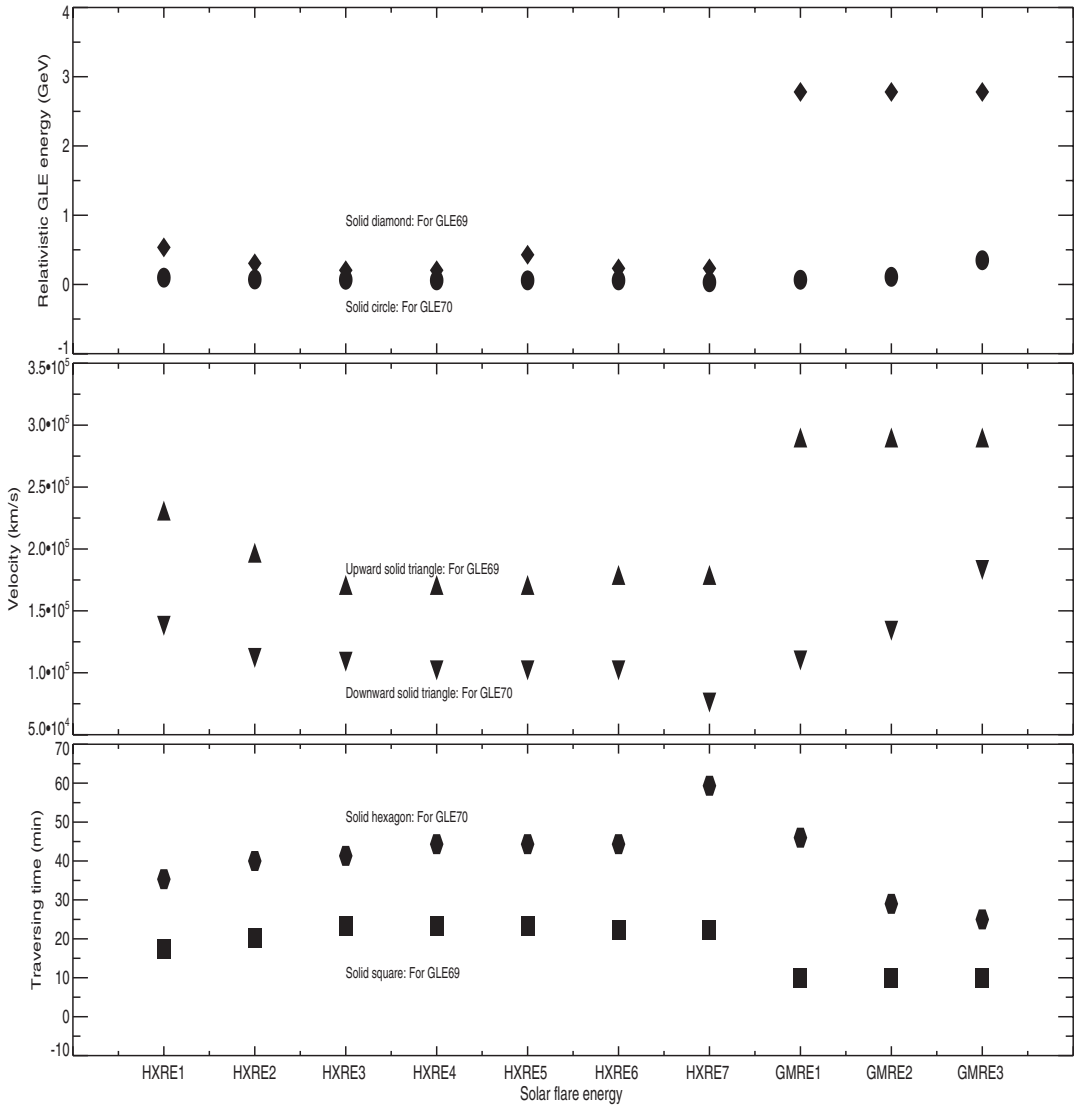

Figure 5. Solar flare energy bands HXRE1, HXRE2, HXRE3, HXRE4, HXRE5, HXRE6, HXRE7, GMRE1, GMRE2, and GMRE3 indicate hard X-ray flare energy bands (6–12 keV, 12–25 keV, 25–50 keV, 50–100 keV, 100–300 keV, 300–800 keV, 800–7000 keV) and SEP flare energy bands (>30 MeV, >50 MeV, >100 MeV), respectively. Top: the relativistic energy (mid) and the presumed velocity of GLE69 and GLE70 are exhibited. Accordingly, (bottom) the traversing time of GLE69 and GLE70 particles along spiral magnetic field lines are also displayed. Using the nominal path lengths deduced by Reames (2009a), the velocity of the particle has been determined by Equation (1) and relativistic energies of the GLE69 and GLE70 particles have been computed by means of Equation (2). Here we consider that the γ-ray flares >30 MeV may cause GLE69 because there seems to be particle acceleration that causes GLE >1 GeV. On the contrary, GLE70 might have been caused by some other solar agent (e.g., CME-driven shock) or by a much higher energy gamma-ray flare. (SEP flares with energy higher than 100 MeV are not found for these two events.)

the fact that the higher speed particle takes less time to traverse along the Archimedean spiral magnetic field lines. We may imply that the closer the time integration between the flare and GLE is, the more effective the released energy from accelerated particles in the solar flare is because, as seen, the same energy band of the flare has a higher peak increase rate in GLE69 than in GLE70 and other components followed a similar trend. This gives an otherwise implicit sense that the GLE and solar flares of different energy bands—all of these solar species—originate from the same solar eruption and as they travel along the spiral magnetic field lines, they might be deflected by magnetic field lines or by front-runner CME-driven shocks.

5. GENERAL DISCUSSION

The observational time lag between GLE and the solar flare used to obtain the traversing time of the particle might be contaminated by the recording time delay (the solar flare is recorded in the geostationary orbit, whereas GLE is registered on the surface of the Earth) and so the traversing time of the particle can be something more or less than the accurate time. Another fact is that we used the nominal path length determined by Reames (2009a, 2009b) because all solar erupted species are supposed to travel along the same spiral field lines. The traversing time of the GLE70 particle is found to be very long (>25 minutes) and ultimately the velocity is very low (0.75e5–1.22e5 km s^{-1}), so the particle perhaps traveled a path longer than 1.72 AU. Once we can determine the nominal path length by any alternative means a further refinement on GLE70 will be performed.

The idea of a flare from a high-energy band causing a high-energy particle event/GLE does not seem to suit the terms of Equations (3a) and (3b) theoretically as well as observationally because the band of the energy does not specify the intensity; rather it depends on how closely the flare is integrated with

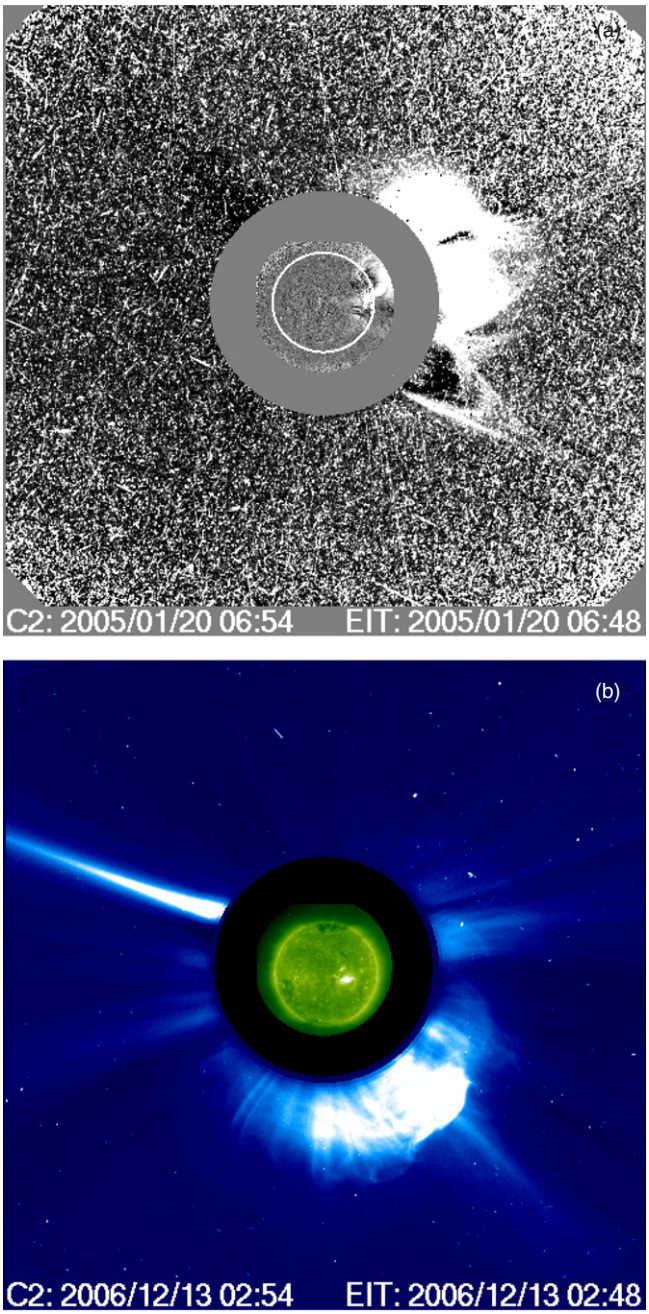

Figure 6. (a) GLE69-associated solar radio emission type II burst concurrent EIT image from the *WIND*-WAVES movie for the Halo CME with height (Rs 30° North) and velocity 882 km s^{-1}. We find that this GLE event does not correspond to the SEP event (see Table 4). (b) GLE70-associated solar radio emission type II burst concomitant EIT image from the *WIND*–WAVES movie for the Halo CME with height (Rs 23° South) and velocity 1773 km s^{-1}. We find that this GLE event corresponds to the SEP event (see Table 4).

(A color version of this figure is available in the online journal.)

GLE. Note that the energy released from vigorously accelerated particles that occasionally occur in solar flare or CME-driven shock fronts might intensify the CRI.

Based on the observation (Section 4.5), the GLE having a peak time difference of ∼2–10 minutes with a concurrent solar flare can be assumed as a prompt GLE and the GLE with a greater peak time difference as a delayed GLE. Accordingly, GLE69 is the prompt GLE event caused by the energy released from the particle acceleration in a high-energy solar flare and GLE70 is a delayed GLE event caused by another acceleration process, possibly CME-driven shocks. In this respect, a few researchers (Firoz et al. 2011a, 2011b) suggested that the shock waves can modulate CRI either directly or inversely, and thus the possibility of the production of GLE70 by shock waves cannot be confirmed. Since the acceleration region of the GLE70-associated solar flare is ∼40° away from the Sun–Earth connecting magnetic field lines (Section 4.2), the particles might undergo considerable azimuthal dispersion to reach the base of those field lines (see mechanisms in Perez-Peraza 1986; Alvarez-Madrigal et al. 1986). Thus, the delayed GLE might be the result of azimuthal transport of solar particles taking place in the solar corona. The alternative process, the particle acceleration in reconnection of the coronal magnetic neutral sheet (MNCS), in which particle energy can reach tens of GeV, might also be the mechanism for a delayed GLE (e.g., Perez-Peraza et al. 2006, 2008).

In fact, GLE is highly anisotropic. Using data from a single Neutron Monitor does not give a concrete idea from which to draw a clear conclusion because if the asymptotic direction of the Neutron Monitor is not aligned with the interplanetary magnetic field, the earliest part of the anisotropic particle beam might not be seen. Therefore, it may be useful to check the anisotropic particle beam and transport effect of the GLE events before analyzing solar flares and/or CMEs/MNCSs in terms of the model of azimuthal particle dispersion.

6. SUMMARY AND CONCLUSION

We pursued a detailed case study on the possible mechanism of GLE69 and GLE70. For this, we analyzed GLE69- and GLE70-associated solar flares/CMEs, and concomitant solar radio bursts. Then we scrutinized the cross-correlations of GLE69 and GLE70 with the simultaneous soft/hard X-ray/SEP flares of different energy bands. Finally, we made an extended effort to understand the possible relativistic energy of GLE. Important results of this study are summarized as follows.

1. The cross-correlations of GLE69 and GLE70 with concurrent hard X-ray solar flares are similar to the derivative forms of soft X-rays (see Table 1 and Figure 4).
2. Correlations of both soft and hard X-ray flares do not vary significantly, and we could not identify whether hard or soft X-ray flares are more responsible. Released energies from both species may induce GLE.
3. The relativistic energy of GLE varies with respect to the time lag in that the greater the time lag is, the lower the relativistic energy of GLE will be. This means that the farther the intensive emissions of the solar flares are, the less effective the released energy from solar flares will be. On this idea, when well correlated with SEP flares, GLE69 has sufficient energy (∼2.78 GeV), which makes us believe that it might be caused by high-energy solar flares, whereas GLE70, having much less relativistic energy (∼0.35 GeV) than a usual high-energy particle event should have (⩾1 GeV), was not likely caused by a solar flare.
4. For GLE69, on average, during the pronounced phase (06:50–07:10 UT) of the type III emission burst, the emission measure was ∼28.1 cm^{-3} while the decay phase otherwise representing the solar radio type II emission burst was ∼18.70 cm^{-3} (Table 4). The most rapid response to particle acceleration in a solar flare representing a solar radio type III emission burst is visible during the GLE69 occurrence. This gives us a sense that the high-energy

solar flare associated with the type III burst accelerated the particles whose released energy consequently caused the GLE69.

5. For GLE70, on average, during the intensive phase (02:30–3:00 UT) of the type III emission burst, the emission measure was $\sim$12.60 cm^{-3}, whereas the decay phase otherwise representing the solar radio type II emission burst was $\sim$12.03 cm^{-3} (Table 4). Thus, the speed (1773 km s^{-1}) of the type II radio burst concomitant CME, emission measure ($\sim$12.03 cm^{-3}) and image structures (Figures 6(a) and (b)) demonstrate that the energy released from the particle accelerations in the CME-driven shock front might be the possible mechanism for GLE70. (This cannot be confirmed because we could not determine possible relativistic energy in terms of shocks.)

From this study, it is quite clear that GLE maintains the highest correlations with solar flares, but the highest correlations do not imply unambiguously that GLE can be caused by a solar flare. The main criterion is to recognize the relativistic energy of the GLE particle. The released energy from the accelerated particles in the solar flare maintaining the lowest time lag can raise the possible relativistic energy of GLE $\geqslant$1 GeV. This sort of solar flare can be considered as the cause of the GLE occurrence.

We are grateful to the anonymous reviewer for constructive comments that indeed improved the quality of the paper. Thanks to the PIs of *RHESSI*/*GOES*/*WIND*-WAVES/RSTN/*Yohkoh*/NOAA/ONM for providing observational data. Special thanks to Professor Brian R. Dennis and Dr. Kim Tolbert for explaining *RHESSI* instrumentations and commands under the SSW workbench. This work has been financed by the WCU Program (No. R31-10016) through the National Research Foundation of the Republic of Korea funded by the Ministry of Education, Science, and Technology and by the Korea Research Foundation Grant (KRF-2008-314-C00158, 20090071744, and 20100014501) funded by the Korean Government (MOEHRD, Basic Research Promotion Fund). K.K. is supported by VEGA grant agency project 2/0081/10.

REFERENCES

Alania, M. V., Iskra, K., & Siluszyk, M. 2009, Adv. Space Res., 45, 1203
Alvarez-Madrigal, M., Miroshnichenko, L. I., Perez-Peraza, J., & Rivero-Garduso, F. 1986, SvA, 30, 690
Aschwanden, M. J. 2006, Physics of the Solar Corona: an Introduction (Chichester: Praxis)
Aschwanden, M. J. 2011, Space Sci. Rev., in press, arXiv:1005.0029v1
Aschwanden, M. J., Benz, A. O., Dennis, B. R., & Schwartz, R. A. 1995, ApJ, 455, 347
Berezhko, E. G., & Taneev, S. N. 2003, Astron. Lett., 29, 530
Bombardieri, D. J., Duldig, M. L., Humble, J. E., & Michael, K. J. 2008, ApJ, 682, 1315
Cane, H. V., & Erickson, W. C. 2003, J. Geophys. Res. A5, 108, 1203
Chupp, E. L., Trottet, G., Dunphy, P. P., & Rieger, E. 2003, in Proc. 28th International Cosmic Ray Conf., ed. T. Kajita et al. (Tokyo: Universal Academy Press), 3171
Cliver, E. W. 2006, ApJ, 639, 1206
Cliver, E. W., Kahler, S. W., Shea, M.A., & Smart, D. F. 1982, ApJ, 260, 362
Dennis, B. R. 1985, Solar Phys., 100, 465
Dennis, B. R., Phillips, K. J. H., Sylwester, J., et al. 2005, Adv. Space Res., 35, 1723
Dorman, L. I. 1957, Gostekhteorizdat, Moscow (in Russian), Engl. Transl. in 1958, Cosmic Ray Variations (Wright-Patterson Air Force Base, OH, Cosmic Ray Variations)
Dorman, L. I. 1963, in Progress in Physics of Cosmic Rays and Elementary Particles, Vol. 7, ed. J. G. Wilson & S. A. Wouthuysen (Amsterdam: North-Holland), 320
Dorman, L. I. 2004, Cosmic Rays in the Earth's Atmosphere and Underground (Dordrecht: Academic)
Dorman, L. I. 2006, Cosmic Ray Interactions, Propagation, and Acceleration in Space Plasmas, (Dordrecht: Springer)
Dorman, L. I. 2010, Solar Neutrons and Related Phenomena, (Dordrecht: Springer)
Dorman, L. I., & Miroshnichenko, L. I. 1968, Fizmatgiz, Moscow (in Russian), Engl. Transl. in 1976, Solar Cosmic Rays (Washington, DC: NASA)
El-Borie, M. A. 2003, Astropart. Phys., 19, 549
Firoz, K. A. 2006, in WDS: Part II: Physics of Plasmas and Ionized Media, ed. J. Safrankova & J. Pavlu (Prague: Charles Univ. MATFYZPRESS), 33
Firoz, K. A. 2008, in WDS: Part II: Physics of Plasmas and Ionized Media, ed. J. Safrankova & J. Pavlu (Prague: Charles Univ. MATFYZPRESS), 183
Firoz, K. A., Cho, K.-S., Hwang, J., et al. 2010, J. Geophys. Res, 115, A09105
Firoz, K. A., Hwang, J., Dorotovič, I., Pintér, T., & Kaushik, S. C. 2011a, Ap&SS, 331, 469
Firoz, K. A., & Kudela, K. 2007, in WDS: Part II: Physics of Plasmas and Ionized Media, ed. J. Safrankova & J. Pavlu (Prague: Charles Univ. MATFYZPRESS), 106
Firoz, K. A., Kumar, P., & Cho, K.-S. 2009, Ap&SS, 325, 185
Firoz, K. A., Moon, Y.-J., Cho, K.-S., et al. 2011b, J. Geophys. Res., 116, A04101
Gallagher, P. T., Moon, Y. J., & Wang, H. 2002, Solar Phys., 209, 171
Kahler, S. W., Reames, D. V., & Sheeley, N. R., Jr. 2001, ApJ, 562, 558
Kahler, S. W., Simnett, G. M., & Reiner, M. J. 2003, in Proc. 28th International Cosmic Ray Conf., ed. T. Kajita et al. (Tokyo: Universal Academy Press), 3415
Kane, R. P. 2009, Rev. Bras. Geofis., 27, 165
Kudela, K., & Usoskin, I. 2004, Czech J. Phys., 54, 239
Kumar, P., Srivastava, A. K., Somov, B. V., Manoharan, P. K, Erdelyi, R., & Uddin, W. 2010, ApJ, 723, 1651
Kurt, V. G., Yuhkov, B. Y., Kudela, K., & Galkin, V. I. 2010, Cosm. Res., 48, 70
Kuznetsov, S. N., Kurt, V. G., Yushkov, B. Yu, et al. 2006, Contrib. Astron. Obs. Skalnate Pleso, 36, 85
Lin, R. P., Dennis, B. R., Hurford, G. J., et al. 2002, Sol. Phys., 210, 3
MacDowall, R. J., Lara, A., Manoharan, P. K., et al. 2003, J. Geophys. Res. Lett. 0, 30, 8018
MacDowall, R. J., Richardson, I. G., Hess, R. A., & Thejappa, G. 2009, in IAU Symp 257, Universal Heliophysical Processes, ed. N. Gopalswamy & D. F. Webb (Cambridge: Cambridge Univ. Press), 335
Mavromichalaki, H., Plainaki, C., Gerontidou, M., et al. 2007, IEEE Trans. Nucl. Sci., 54, 1082
Mavromichalaki, H., Souvatzoglou, G., Sarlanis, C., et al. 2010, New Astron., 15, 744
Miroshnichenko, L. I. 2001, Solar Cosmic Rays (Dordrecht: Kluwer)
Moon, Y.-J., Choe, G. S., Wang, H., et al. 2002, ApJ, 581, 694
Neupert, W. M. 1968, ApJ, 153, L59
Perez-Peraza, J. 1986, Space Sci. Rev., 44, 91
Perez-Peraza, J., Gallegos-Cruz, A., Vashenyuk, E. V, Balabin, Y. V., & Miroshichenko, L. I. 2006, Adv. Space Res., 38, 418
Perez-Peraza, J., Vashenyuk, E. V., Gallegos-Cruz, A., Balabin, Y. V., & Miroshichenko, L. I. 2008, Adv. Space Res., 41, 947
Plainaki, C., Belov, A., Eroshenko, E., Mavromichalaki, H., & Yanke, V. 2007, J. Geophys. Res., 112, A04102
Reames, D. V. 1999, Space Sci. Rev., 90, 413
Reames, D. V. 2009a, ApJ, 693, 812
Reames, D. V. 2009b, ApJ, 706, 844
Reames, D. V., & Lal, N. 2010, ApJ, 723, 550
Reiner, M. J., Krucker, S., Gary, D. E., et al. 2007, ApJ, 657, 1107
Ryan, J. M., Lockwood, J. A., & Debrunner, H. 2000, Space Sci. Rev., 93, 35
Velinov, P., & Mishev, A. 2008, in Proc. 30th International Cosmic Ray Conf., Vol. 1, ed. R. Caballero et al. (Tokyo: Universal Academy Press), 749
Veronig, A., Vrsnak, B., Dennis, B. R., et al. 2002, in Proc.10th European Solar Physics Meeting, Solar Variability: From Core to Outer Frontiers, ed. A. Wilson (ESA SP-506; Noordwijk: ESA), 367
Wang, R., & Wang, J. 2006, Adv. Space Res., 38, 489
Wang, Y., Xue, X., Shen, C., et al. 2006, ApJ, 646, 625
Warren, H. P., & Antiochos, S. K. 2004, ApJ, 611, L49
Wild, J. P., Smerd, S. F., & Weiss, A. A. 1963, ARA&A, 1, 291
Yashiro, S., Gopalswamy, N., Michalek, G., et al. 2004, J. Geophys. Res., 109, A07105